Welcome   Comments   Help

Microstructural evolution of dense and porous pyroelectric Pb$_{1-x}$Ca$_x$TiO$_3$ thin films

Andreas Seifert, Laurent Sagalowicz, Paul Muralt, and Nava Setter
Laboratoire de Céramique, Département des Matériaux, Ecole Polytechnique Fédérale de Lausanne, 1015 Lausanne, Switzerland

Pb$_{1-x}$Ca$_x$TiO$_3$ thin films with $x = 0$–0.3 for pyroelectric applications were deposited on platinized silicon wafers by chemical solution processing. Ca-substitution for Pb in PbTiO$_3$ results in a reduced c/a ratio of the unit cell, which, in turn, leads to better pyroelectric properties. Control of nucleation and growth during rapid thermal annealing to 650 °C allowed the formation of either highly porous or dense (111) oriented films. The inclusion of pores creates a matrix-void composite with the low permittivity desired for pyroelectric applications, resulting in a high figure of merit. The growth mechanisms for the microstructural evolution of both dense and porous films were analyzed by x-ray diffraction, transmission electron microscopy, scanning electron microscopy, and Rutherford backscattering spectrometry and allowed establishment of microstructure/property relationships.

I. INTRODUCTION

Pyroelectric thin films in point detectors and arrays have many applications in temperature sensing systems for fire- and intruder-detection, air condition control, and thermal imaging.[1,2] The advantage of thin-film devices over bulk materials is that they exhibit low heat capacity and thus low thermal time constants which is especially important for high frequency imaging. Also, thin films can be directly deposited on platinized silicon to allow direct integration with electronics. Lead titanate (PT) is a well-known tetragonal perovskite pyroelectric material with a very large spontaneous polarization of $P_s = 81 \ \mu$C/cm^2 and a high Curie temperature of $T_C \approx 490$ °C. Smaller cations like Ca^{2+} have been used as *A*-site dopants in order to obtain higher pyroelectric coefficients $p = dP_s/dT$ by lowering the Curie temperature (e.g., 15% Ca: $T_C = 370$ °C).[3]

Highly (001)-oriented Pb$_{1-x}$Ca$_x$TiO$_3$ (PCT) films would be ideal for pyroelectric applications because P_s is perpendicular to the substrate. However, because the thermal expansion coefficient of silicon is much lower than the one of the films, tensile stress builds up during cooling from the processing temperature. This causes the c-axis to rotate into the film/substrate plane to compensate the stress, and mostly (100) oriented films result which are not useful for pyroelectric applications. Therefore (111) oriented films are advantageous, where 58% of P_s can be achieved normal to the substrate.[4] To evaluate the quality of a pyroelectric material, different figures of merit exist, depending upon the device requirements. For good voltage response[1,5] it is necessary to maximize p and lower the permittivity, ϵ_r, to increase the figure of merit $F_V = p/\epsilon_r$. For high detectivity (signal-to-noise ratio) the dielectric loss, tan δ, becomes important and the figure of merit is $F_D = p/\sqrt{\epsilon_r \tan \delta}$.[6] The possibility of lowering ϵ_r by incorporation of void space into the films has been explored in this study by forming a matrix-void composite[7] with reduced permittivity.

Chemical solution deposition has been used for the processing of the PCT thin films.[8] The original method for the synthesis of PT double alkoxide precursors[9] was modified by reaction with a Ca-acetate/glacial acetic acid solution. Due to the reduced shelf life of these solutions (about three weeks), stable precursors based on 1,3-propane diol were also synthesized.[10] Both precursor types were used for film processing and compared with respect to their decomposition behavior as well as their resulting microstructures and properties. Porous microstructures can be fabricated due to the particular phase evolution of lead-based perovskites processed from solution precursors. It is well-known that under certain conditions the crystallization of perovskite during sol-gel processing takes place via an intermediate, metastable Pb–Ti–fluorite (or pyrochlore).[11–14] Control of the nucleation kinetics allows the conservation of the polycrystalline porous fluorite microstructure during the phase transformation to perovskite and thus the formation of thin films with the desired low permittivity and high pyroelectric coefficients. The purpose of this paper is to determine the different growth mechanisms for the evolution of dense and porous microstructures and to relate these to the dielectric and pyroelectric properties observed.

II. EXPERIMENTAL PROCEDURE

Two different solution precursor systems were used for the deposition of the Pb$_{1-x}$Ca$_x$TiO$_3$ films: modified

metal-alkoxide precursors as well as 1,3-propane diol-based solutions were synthesized.

During the alkoxide-synthesis, based on the route introduced by Gurkovich and Blum,[9] the precursor was modified by the addition of a Ca-acetate solution in acetic acid. Pb(CH$_3$COO)$_2$ × 3.03 H$_2$O was dissolved in 2-methoxy ethanol (ME), dehydrated by vacuum-distillation at 0.3 atm and 130 °C (Büchi AG, Rotavapor EL 141, Flawil, Switzerland), and subsequently redissolved in anhydrous 2-methoxy ethanol. Previously assayed Ca(CH$_3$COO)$_2$ × 0.11 H$_2$O was dissolved in glacial acetic acid at 70 °C. Following this, the Pb-acetate/2-methoxy ethanol solution and a Ti-isopropoxide/2-methoxy ethanol-mixture were added to the Ca-acetate solution under nitrogen. Refluxing at 120 °C at 0.5 atm for 90 min yielded the modified alkoxide precursor. The precursor concentration was adjusted to 0.4 molar by final vacuum-distillation at 0.3 atm and 130 °C. Four vol% of formamide were added as drying control agent.[15] The precursors prepared by this method had a shelf life of three weeks before the appearance of a Ca-containing precipitate.

The solutions based on 1,3-propane diol (PD) as solvent[10,16] are not moisture sensitive, have a much longer shelf life (> one year), and it has been shown for Pb(Zr, Ti)O$_3$ that thick layers up to 3 μm on silicon and 10 μm on sapphire can be obtained in a relatively small number of coating steps.[17] For this synthesis, Pb-acetate hydrate was dissolved in 1,3-propane diol in a molar ratio of Pb^{2+}/1, 3-propane diol = 1 − x/5 and refluxed at 110 °C for one hour. Ti-di-isopropoxide-bis-acetylacetonate (75% in 2-propanol) in a molar ratio of Pb^{2+}/Ti^{4+} = 1 − x/1 was added to the solution after cooling to 80 °C. Reaction was induced during refluxing at 115 °C for 2 h. About 80% of the reaction by-products (mostly 2-propanol originating from Ti-di-isopropoxide-bis-acetylacetonate and its solvent) were removed by distillation at 120 °C. Cooling to room temperature allowed the addition of an aqueous Ca(CH$_3$COO)$_2$ × 0.11 H$_2$O solution with a molar ratio of Ca^{2+}/Ti^{4+} = x/1 and H$_2$O/1,3-propane diol = 5/1 (1,3-propane diol as used for Pb-acetate solution). Initial precipitates dissolved after stirring for several hours at room temperature, resulting in clear yellow liquids with a molarity of ∼0.8.

Thermal gravimetric analysis (TGA) and differential scanning calorimetry (DSC, Mettler-Toledo, 86060 Greifensee, Switzerland) were used to characterize the pyrolysis and crystallization behavior of the two precursor systems. For this purpose the solution precursors were dried on a hotplate at 60 °C for three hours, ground to powder, and heated at 10 °C/min to 550 °C during the thermal analysis. For PCT25 a high temperature TGA/DSC run was performed to 800 °C, and mass spectrometry was carried out to analyze the evolving gas.

Film deposition by spin-coating (Headway Research Inc., Garland, TX, USA) was carried out at 2000–3000 rpm for 40 s on in-house platinized silicon substrates with a TiO$_2$ adhesion layer between SiO$_2$ and Pt. A 2 nm TiO$_2$ nucleation layer was used to achieve a preferred (111) orientation of the PCT films.[4] After each deposition the films derived from ME- or PD-based precursors were pyrolyzed for 15 or 40 s, respectively, at 350 °C on a hotplate. Final heat-treatment of stacks of 2–8 layers at 650 °C for 5 min was carried out in a rapid thermal anneal apparatus using heating rates of 1, 6, and 60 °C/s (RTA, Process Product Corp., Andover, MA, USA). During fast heating an overshoot over the programmed temperature occurs and is taken into account for the processing temperatures indicated. The thickness of individual layers from ME- and PD-based precursors was ∼70 and ∼250 nm, respectively. Most films were made to a final thickness of ∼0.5 μm.

TEM and XRD studies were carried out to understand the evolution of the different microstructures in dependence of the heating rate. Two series of samples were prepared after pyrolysis at 350 °C: One series where the samples were heated at 60 °C/s to 345 °C (pyrolysis at 300 °C), 370 °C (pyrolysis at 300 °C), 400 and 420 °C. For the second series the slower heating rate of 1 °C/s was used for heating to 350, 400, 500, 525, 550, and 600 °C, all pyrolyzed at 350 °C. All samples were held for 15 s before free cooling to room temperature. Additionally, three films were prepared and analyzed as pyrolyzed at 300, 325, and 350 °C.

For electrical characterization circular Cr/Au (10 nm/300 nm) top electrodes of 0.6 mm diameter were deposited by evaporation through a shadow mask (Edwards, West Sussex, GB). Profilometer thickness measurements (α-Step 260, Tencore, Mountain View, CA, USA) and bottom electrode contact was permitted by etching a part of the PCT layer in a HF/HCl/H$_2$O mixture. A multi-frequency LCR-meter (Hewlett-Packard 4274A, Palo Alto, CA, USA) was used to determine dielectric loss, tan δ, and to measure capacities in order to calculate the permittivities, ϵ_r, of the films. Pyroelectric currents were measured dynamically as a function of a 1 °C temperature change, controlled by a wave-form generator driven Peltier element.[18,19] In order to achieve high pyroelectric coefficients, p, the films were poled on a hotplate for 10 min at temperatures between 150 and 200 °C and fields between 200 and 700 kV/cm. The poling field necessary to achieve an optimized pyroelectric coefficient was determined experimentally by systematically increasing the field strength and temperature until no further improvement of p and F could be measured. Field emission scanning electron microscopy (SEM; JEOL, 6300F, Tokyo, Japan), transmission electron microscopy (TEM; Phillips, EM430, Eindhoven, Holland; Hitachi HF2000,

Tokyo, Japan) and x-ray diffraction (XRD; Siemens, D500, Munich, Germany), as well as Rutherford back-scattering spectrometry (RBS) were used for microstructural characterization of the films.

III. RESULTS

A. X-ray diffraction

Powders of the same precursors used for film deposition were made by drying, pyrolysis, and crystallization of the solutions in a conventional furnace at 650 °C. XRD scans showed that the powders consisted of phase pure Pb$_{1-x}$Ca$_x$TiO$_3$ perovskite for $x = 0$–0.3. The lattice parameters of the PCT powders as given in Table I were corrected with a silicon internal standard and determined by a least squares refinement. XRD scans were also used to evaluate phase purity of PCT thin films of the same composition. For all films, the observed reflections could be attributed to the perovskite phase of PCT, Pt, and Si. XRD scans were also performed for the study of the microstructural evolution as a function of the heating rate. The results are given in Sec. C.

B. TGA and DSC

TGA and DSC analysis of pyrolysis and crystallization were performed on powders of both precursor types. The TGA/DSC scan at 10 °C/min to 550 °C in Fig. 1(a) for the ME-based PCT20 precursor shows advantageous weight loss properties. At 350 °C the weight loss of the powder is to ∼ 98% complete which coincides with a first decomposition/crystallization peak that has its maximum at 340 °C. The onset of Pb$_{0.80}$Ca$_{0.20}$TiO$_3$ perovskite crystallization is at 492 °C with its maximum at 503 °C. As it is known that in PbTiO$_3$-based systems an intermediate metastable phase with a pyrochlore or fluorite structure crystallizes first,[11–14] several additional heating/holding experiments were carried out in an attempt to separate the decomposition of the precursor and the crystallization to the intermediate phase. However, no peak separation could be found in any of the experiments, suggesting a temperature overlap of the two phenomena.

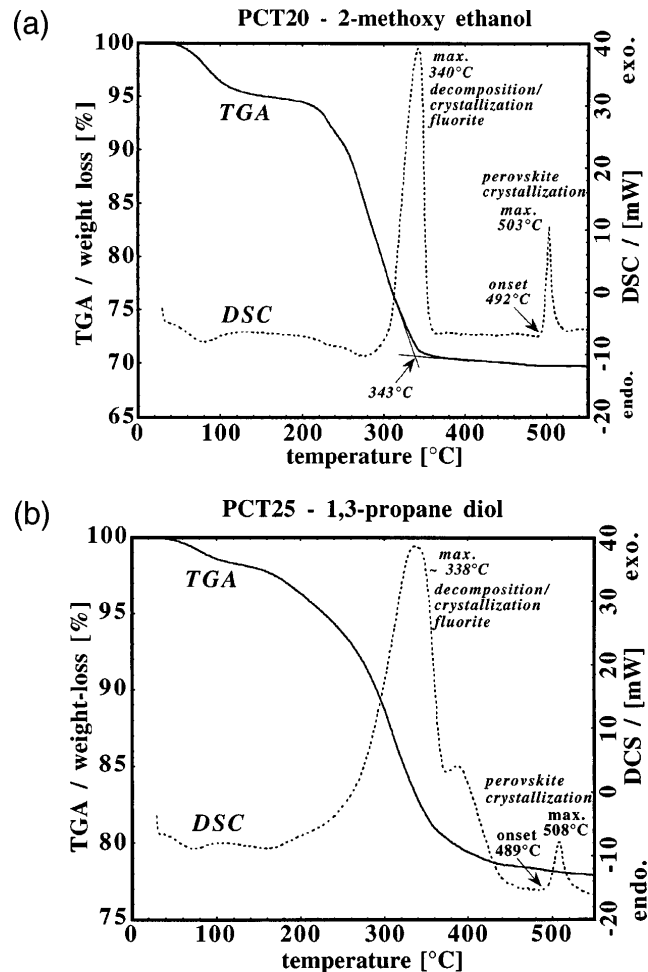TGA/DSC analysis of a PD-based PCT25 precursor, shown in Fig. 1(b), reveals a less abrupt weight loss. The

FIG. 1. (a) TGA/DSC of a 2-methoxy ethanol-based PCT20 precursor. (b) TGA/DSC of a 1,3-propane diol based PCT25 precursor.

weight loss of the dried powder is ∼ 82% at 350 °C and continues at a low rate to temperatures above 550 °C. The first DSC decomposition/crystallization peak occupies a broader temperature range than in the case of the ME precursor, but its peak temperature of 338 °C is almost the same. Nearly the same temperatures as compared to the ME precursor were measured for the onset and maximum of perovskite crystallization which are at 489 and 508 °C, respectively, explaining the observed similarities of microstructures and properties. Further TGA and DSC experiments to separate the DSC decomposition/crystallization peak and to determine the origin of the shoulder were carried out. Intermediate holding times of 290 and 360 °C allowed observation of two separate phases of weight loss, resulting in the shoulder. As in the case of the ME-based precursor, the decomposition may coincide with the crystallization peak of the intermediate phase.

A high temperature TGA/DSC experiment to 800 °C for PCT25 (PD-based precursor) showed an additional

TABLE I. Powder lattice parameters obtained by least squares refinement after correction with Si standard.

Composition	a (Å)	c (Å)
PbTiO$_3$	3.9046 (3)	4.1498 (6)
Pb$_{0.85}$Ca$_{0.15}$TiO$_3$	3.9081 (4)	4.1135 (7)
Pb$_{0.80}$Ca$_{0.20}$TiO$_3$	3.8905 (6)	4.074 (1)
Pb$_{0.75}$Ca$_{0.25}$TiO$_3$	3.8834 (7)	4.044 (1)
Pb$_{0.70}$Ca$_{0.30}$TiO$_3$	3.8928 (5)	4.0295 (7)

weight loss of 0.43% at about 720 °C and a CO_2 peak in the mass spectrum.

C. Effect of the heating rate on the microstructural development

$Pb_{1-x}Ca_xTiO_3$ films with $x = 0$, 0.05, 0.1, 0.15, 0.2, 0.25, and 0.3 were ramped to 650 °C at 1, 6, or 60 °C/s. The heating rate was found to have a profound effect on the microstructural development of the films. PCT films were deposited (2 layers for PD, 5 layers for ME), pyrolyzed, and subsequently cleaved into two halves for heat treatments at different RTA heating rates. Cross section SEM of an ME-derived $Pb_{0.70}Ca_{0.30}TiO_3$ film shows that the first half, heated at 60 °C/s in Fig. 2(a) has a dense microstructure with relatively large columnar grains, reaching from the Pt bottom electrode to the top of the film. The film thickness was measured as 290 nm, both by SEM and profilometry. The second half of the film, heated much slower at 1 °C/s, resulted in a different microstructure with a much lower density and an average pore and grain size of around 30 nm, as shown in Fig. 2(b). On the surface of this film, as well as on all others observed by SEM, a layer with a different microstructure is present, which probably results from surface nucleation. The film thickness was measured by SEM and profilometry as ~380 nm. Assuming that the film with the heating rate of 60 °C/s in Fig. 2(a) has achieved theoretical density, the pore volume in the more slowly heated film [Fig. 2(b)] would amount to ~25%. To confirm this observation, density measurements by Rutherford backscattering spectrometry were carried out for films with various Ca concentrations (Sec. D). The amount of porosity in the layers can also be calculated from the measurement of dielectric properties (Sec. E).

Image analysis of SEM micrographs of PCT films of different compositions all heated to 650 °C showed that the average grain and pore sizes decrease with increasing Ca content. For $PbTiO_3$ a value of ~82 nm was found, whereas grains of PCT30 films had a diameter of only ~30 nm. These results, considering the higher melting temperatures of Ca-rich compositions, are shown in Fig. 3 for grain size versus the ratio of the heat-treatment temperature over the homologous melting temperatures, $T_{heat-treat.}/T_{melt}$.

TEM and XRD were used to study the evolution of the different microstructures as a function of the heating rate for two series of PCT25 samples (PD-based precursor), one heated at 60 °C/s and the other at 1 °C/s.

XRD results of both, a sample heated to 345 °C at 60 °C/s (pyrolysis at 300 °C) and a sample pyrolyzed at 300 °C indicate amorphous material, as shown in Fig. 4(a). The first perovskite reflections are observed after heating to 370 °C. Cross-section TEM of the 345 °C
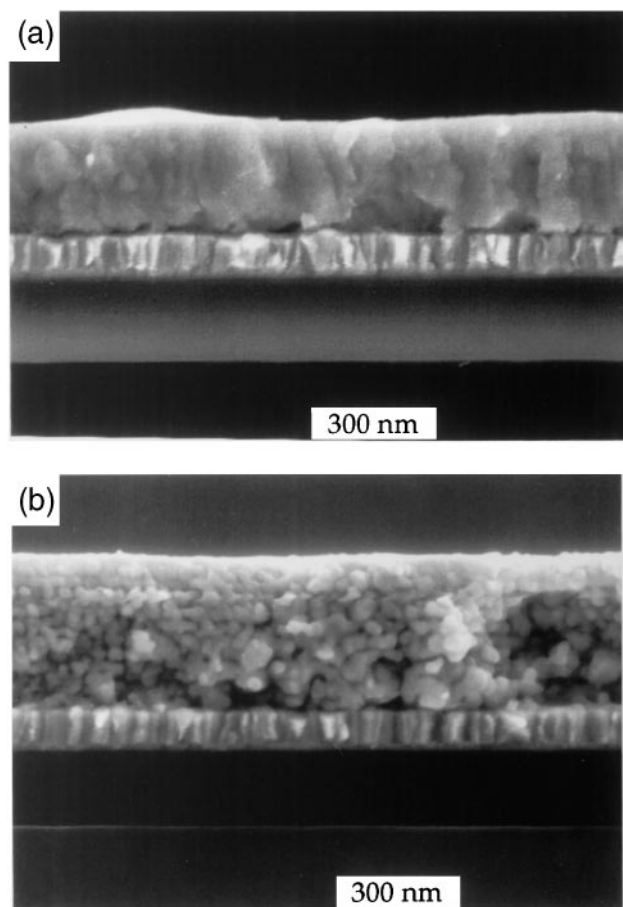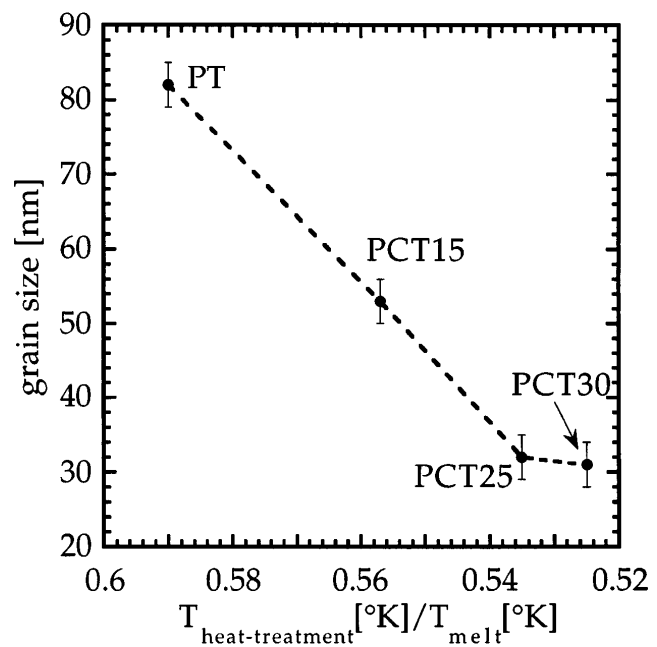

FIG. 2. (a) Cross-section SEM of a dense PCT30 film, heated at 60 °C/s to 650 °C. (b) Cross-section SEM of a porous PCT30 film, heated at 1 °C/s to 650 °C.

FIG. 3. Grain size versus the homologous $T_{heat-treat.}/T_{melt}$ of different PCT compositions for porous films heated at 1 °C/s.
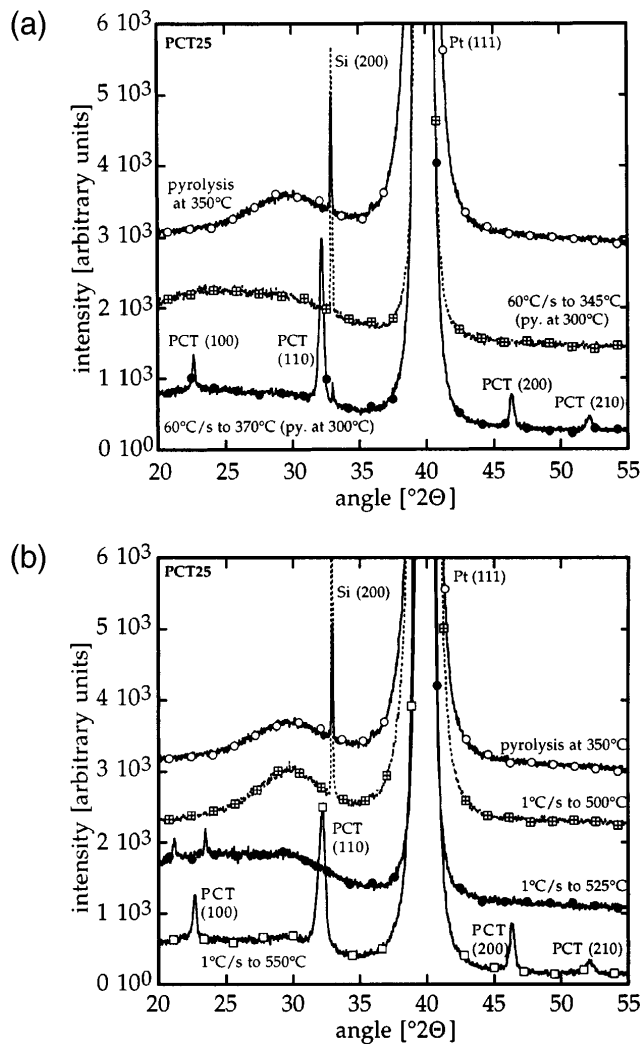
FIG. 4. (a) X-ray diffraction of PCT15 thin films heated at 60 °C/s. (b) X-ray diffraction of PCT15 thin film heated at 1 °C/s.
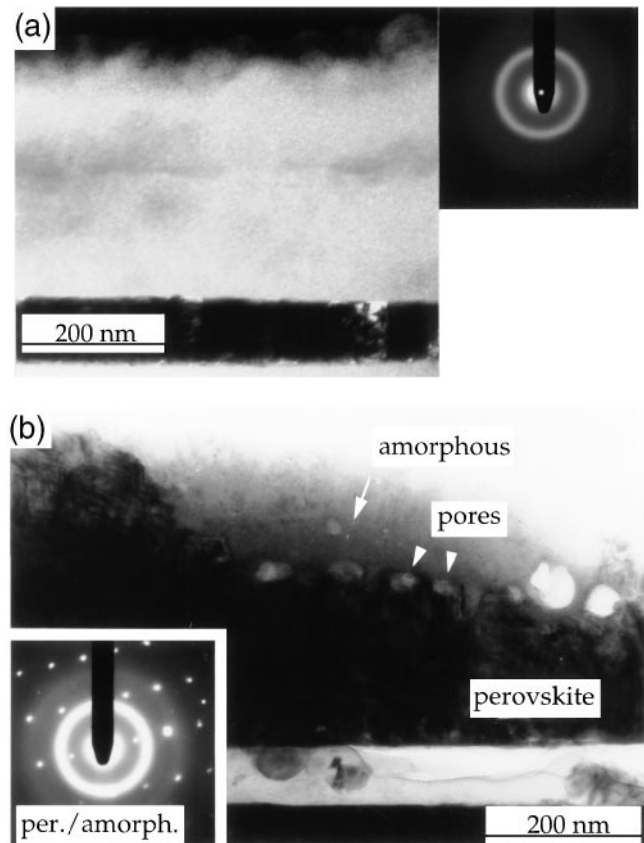

FIG. 5. (a) TEM BF image with SADP of an amorphous PCT15 film heated at 60 °C/s to 345 °C. (b) TEM BF image with SADP of PCT15 perovskite grains growing into an amorphous matrix after heating at 60 °C/s to 370 °C.

sample confirms the amorphous character of the layer as shown in the bright-field (BF) image in Fig. 5(a) with its corresponding small area diffraction pattern (SADP). If the heating temperature is increased to 370 °C at 60 °C/s, BF-TEM shows columnar perovskite grains growing into amorphous material [Fig. 5(b)]. At the interface between the amorphous and the perovskite phase an array of pores can be observed. An intermediate pyrochlore or fluorite phase could not be detected for samples heated at 60 °C/s.

XRD of samples heated at 1 °C/s to 450, 500, and 525 °C, as well as a film pyrolyzed at 350 °C showed a broad reflection at ~30° 2Θ, indicating amorphous or very fine-grained material. Sharp reflections of a fluorite or pyrochlore phase were not seen by XRD and first perovskite reflections occur at 550 °C [Fig. 4(b)]. However, careful TEM analysis showed that for heating to 500 °C an intermediate fluorite phase with grains of

~6 nm diameter is present, as shown in Fig. 6(a) with its respective SADP. The grains grow to about 10 nm after heating to 525 °C. The corresponding SADP in Fig. 6(b) allows indexing for a Pb–Ca–Ti-fluorite with a lattice parameter of ~5 Å. Cross-section TEM of the sample heated at 550 °C shows some surface nucleation of perovskite in a polycrystalline fluorite matrix [see Fig. 6(c)]. The coexistence of fluorite and perovskite was confirmed by electron diffraction. At 575 °C a columnar perovskite structure was observed, and no evidence of fluorite was found.

The determination of the out-of-plane orientation by XRD was complicated by the overlap of the Pt (111) and PCT (111) reflections. Therefore the (111) oriented character of the layers was confirmed by plan-view and cross-section TEM on a sample heated to 600 °C at 1 °C/s. Electron diffraction over large areas in combination with tilting of the plan-view sample shows high intensity for all rings representing reflections of a ⟨111⟩ zone axis like {110}, {220}, and {211}, whereas other rings are of weak intensity, indicating a preferred (111) orientation as shown in Fig. 7(a). In the same figure it can be seen that diffraction over smaller areas
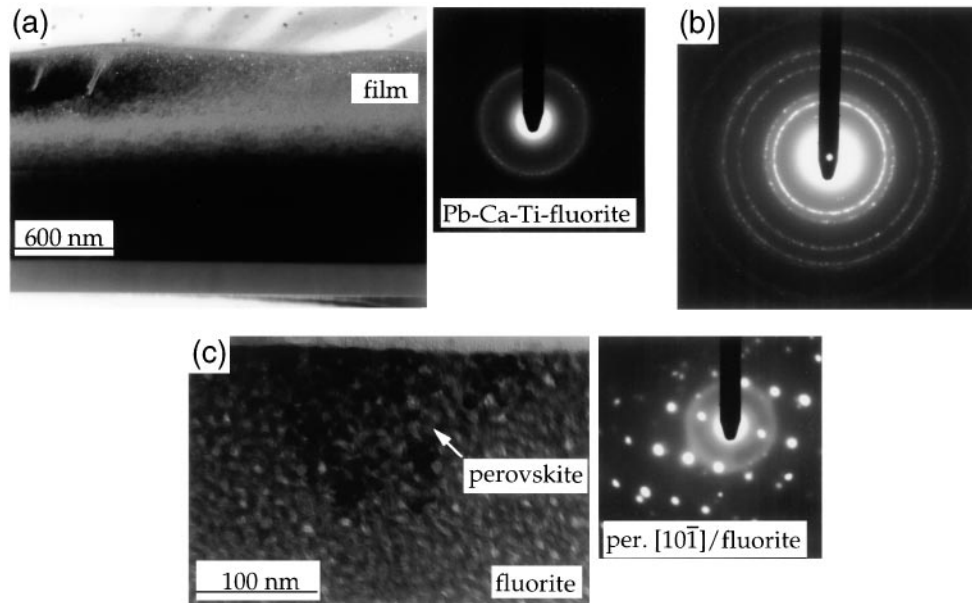
FIG. 6. (a) TEM BF image with SADP of a PCT15 film heated at 1 °C/s that shows Pb–Ca–Ti–fluorite grains with a diameter of ∼6 nm after heating to 500 °C. (b) The SADP of a PCT15 film heated at 1 °C/s to 525 °C can be indexed to a Pb–Ca–Ti–fluorite phase with a lattice parameter of ∼5 Å. (c) TEM BF image with SADP of a PCT15 film heated at 1 °C/s shows perovskite surface nucleation in a matrix of the fluorite phase for heating to 550 °C.

allowed identification of single-crystal-like regions of perfect (111) orientation. Neighboring regions have the same single-crystal-like appearance but are rotated in-plane. Dark-field imaging of a cross-section sample shows columnar perovskite grains, reaching from the platinum bottom electrode to the surface of the film [see Fig. 7(b)].

D. RBS and EDS measurements

For control of the post-processing stoichiometry and for determination of the density of different PCT10 and PCT15 films, RBS depth profiling was carried out (see Table II). In this technique a beam of monoenergetic 2.5 MeV ^{4}He ions is backscattered from the sample to a semiconductor detector with a certain energy loss. For a known thickness, the density of the layers can be directly determined by comparing the measured number of scattering molecules/cm^3 with the theoretical number (e.g., $N_{th} = 1.592 \times 10^{22}$ molecules/cm^3 for PCT10), as shown in Table II. These results correspond to the observations by SEM and calculations based on electrical measurements following Lichteneckers rule as shown below. For confirmation of the post-processing stoichiometry, modeling of the experimental spectra is necessary and shows that the precursor stoichiometry was conserved in the films, as shown in Fig. 8 (the scattering yield cannot be directly related to the microstructure). The simulation is normalized to the platinum of the electrode, and the relative accuracy of the measurement is about 5%.

The same results for the conservation of the post-processing stoichiometry were obtained by TEM-EDS (energy dispersive spectrometry) analysis (Hitachi HF-
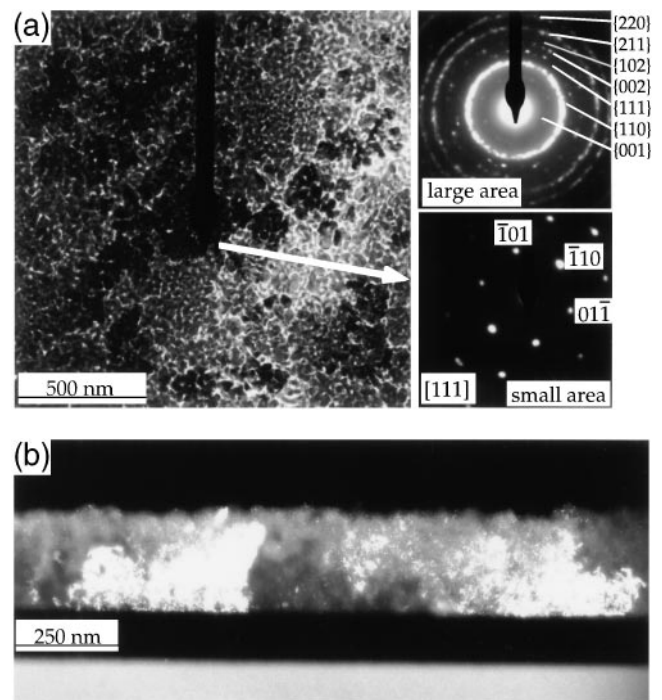

FIG. 7. Confirmation of the (111) orientation of a PCT15 film heated to 600 °C at 1 °C/s: (a) Electron diffraction over large areas of a plan-view sample gives (111) as the preferred orientation. (b) Dark-field imaging of a cross-section sample shows the columnar structure.

TABLE II. Data from RBS depth profiling of dense films (60 °C/s) and porous films (1 °C/s).

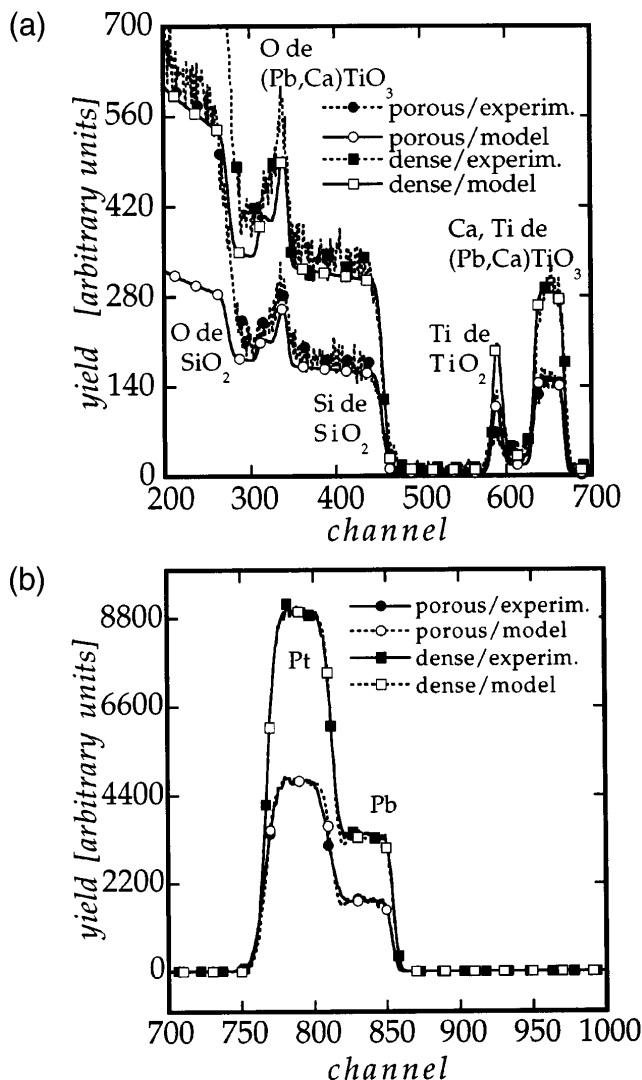| Composition	Heating rate	Film thickness	N [$\times 10^{22}$]	% of N_{th}
Pb$_{0.90}$Ca$_{0.10}$TiO$_3$	1 °C/s	180 nm	1.08	68
Pb$_{0.90}$Ca$_{0.10}$TiO$_3$	60 °C/s	125 nm	1.56	98
Pb$_{0.85}$Ca$_{0.15}$TiO$_3$	1 °C/s	170 nm	1.15	72
Pb$_{0.85}$Ca$_{0.15}$TiO$_3$	60 °C/s	120 nm	1.50	94

FIG. 8. (a) RBS depth profile of a dense and a porous PCT10 film on a Pt/TiO$_2$/SiO$_2$/Si substrate, channel 200–700. (b) RBS depth profile of a dense and a porous PCT10 film on a Pt/TiO$_2$/SiO$_2$/Si substrate, channel 700–1000.

2000, Tokyo, Japan) for PCT15 thin films. The measurements were carried out with liquid nitrogen cooling to avoid beam heating and contamination. An appropriate sample thickness was used to exclude preparation surface effects (especially Pb loss) as well as strong absorption effects. For all measurements standards were used and the results for PCT 15 in atomic percent are as follows:

52% $\pm$ 2 for Ti, 7.5% $\pm$ 0.7 for Ca, and 40% $\pm$ 3 for Pb, where the error represents the standard deviation of the measurement.

E. Electrical characterization

For the electrical characterization, ϵ_r, tan δ, and p were measured before and after poling Pb$_{1-x}$Ca$_x$TiO$_3$ films. The electrical properties of films made from ME- and PD-based precursors were the same for identical compositions and heating rates and will not be treated separately in this section. The dielectric losses at 1 kHz for dense films made by fast heating were tan $\delta \approx$ 0.01–0.025.

Low ϵ_r results from porous films, e.g., 73 for PCT15, whereas dense microstructures of the same composition give high ϵ_r films, e.g., 310. "Lichteneckers rule" gives the permittivity ϵ_m for a mixture of dielectric phases with mixed series and parallel connectivity.[5] Using the measured permittivity of the porous films as ϵ_m, the permittivity of the dense films heated at 60 °C/s as ϵ_2, and the dielectric constant of a gas for the pores in films heated at 1 °C/s as $\epsilon_2 = 1$, the volume fraction V_2 of the porosity can be calculated to 25%, using ln $\epsilon_m = V_1$ ln $\epsilon_1 + V_2$ ln ϵ_2. This value is consistent with SEM and RBS observations.

Poling experiments were carried out to find the lowest possible temperature and electric field strength to achieve a maximum pyroelectric coefficient in combination with a low ϵ_r, and thus high figure of merit, F_V. Figure 9 shows the development of p, ϵ_r, and F_V for a PCT 15 film after 10 min poling (different capacitors for each measurement) either at a constant field of 400 kV/cm with increasing temperature (a), or in dependence of the electric field strength at constant temperature of 170 °C (b). As expected, a plateau for the increase in p and F_V can be found. Choosing poling parameters above the onset of the plateau [~150 °C in (a) and ~600 kV/cm in (b)] leads to increased dielectric loss (>~3%), indicating that the films may be irreversibly damaged in the process. For both poling experiments the resulting permittivity after poling is reduced by 15–20% but nearly constant over a wide range of poling temperatures and fields. The dielectric breakdown strength for films of all compositions was high and breakdown occurred after about 5 min at 160 °C and 1.5 MV/cm.

Figure 10(a) shows the influence of the heating rate on the behavior of the permittivity and the pyroelectric coefficient for PCT20 films. It can be seen that ϵ_r drops significantly with decreasing heating rate, whereas the decrease of the pyroelectric coefficient is much weaker. The behavior of other PCT compositions is similar and was reported elsewhere.[20] Figure 10(b) summarizes the influence of the Ca content on the figure of merit
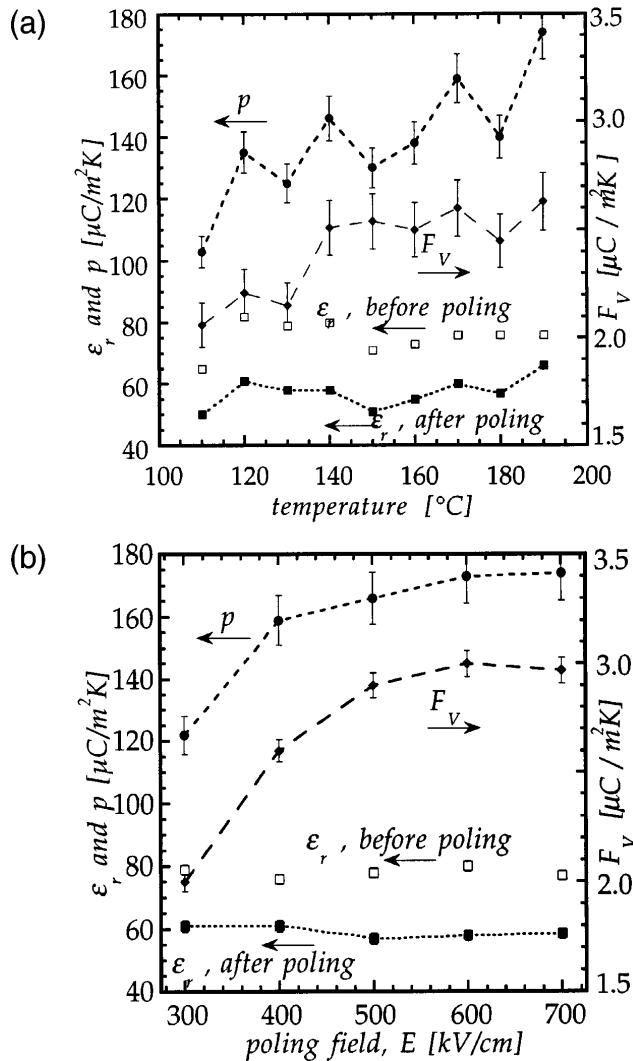
FIG. 9. (a) Poling behavior of a porous PCT15 film at 400 kV/cm for 10 min with increasing temperature. (b) Poling behavior of a porous PCT15 film at 170 °C/10 min and increasing electric field strength.

FIG. 10. (a) Influence of the heating rate on the pyroelectric coefficient p and the permittivity ϵ_r for PCT20. (b) The combination of porous films with a low ϵ_r and the increase of the Ca content lead to higher figures of merit F_V and F_D.

$F_V = p/\epsilon_r$ of porous films. A continuous increase is observed with increasing Ca content with a maximum of $F_V = 3.9$ at 25 mol%.

IV. DISCUSSION

A. Evolution of porous microstructures

The evolution of porous microstructures during slow heating at 1 °C/s is related to the crystallization of an intermediate Pb−Ca−Ti−fluorite phase before perovskite crystallization. This fluorite phase crystallizes throughout the film from the amorphous phase, as it is obtained after pyrolysis. While TEM observations of a sample heated to 500 °C (PD-based precursor) show a polycrystalline porous structure with grains of ∼6 nm diameter [Fig. 6(a)], a sample heated to only 450 °C does not show distinct grains, but readily crystallizes under
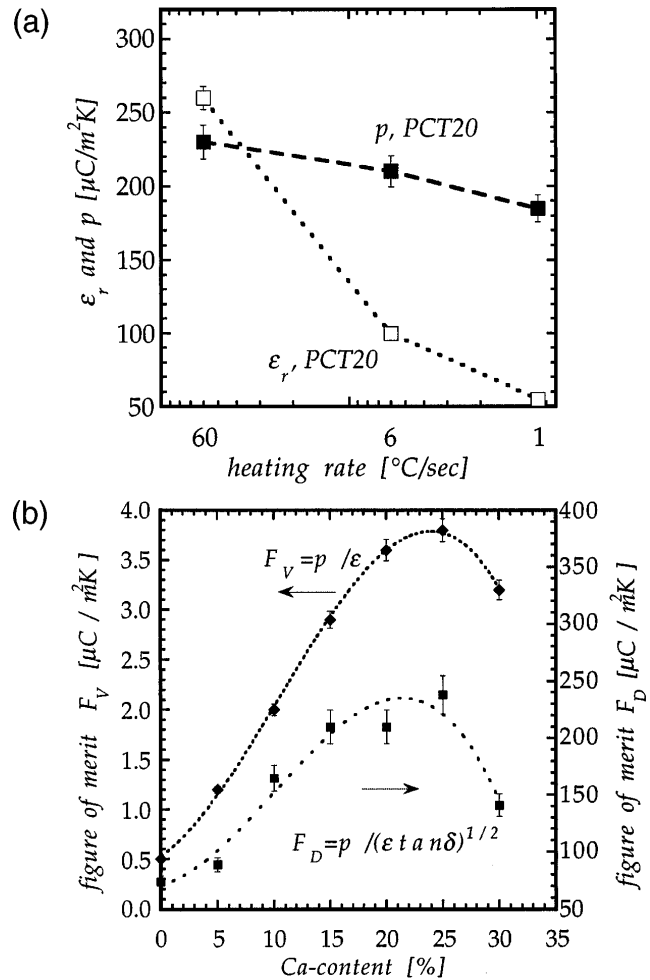
the electron beam during examination, suggesting that critical nuclei are already present at this temperature. The nucleation temperature is therefore likely in the range of 400−450 °C. The shift of the crystallization temperature to lower values for the films of the TEM study as compared to DSC experiments can be expected due to the six times higher heating rate (1 °C/s) employed for the processing of the films. Both observations indicate that nucleation and growth of Pb−Ca−Ti−fluorite occurs in a regime where TGA still shows weight loss from burnout of organics.

X-ray diffraction did not show sharp reflections for the Pb−Ca−Ti−fluorite because of peak broadening due to the small grain size of only ∼6 nm, as observed by TEM for a sample heated to 500 °C. In the x-ray scans only the strongest fluorite reflection in the spectrum, (111), causes a wide peak at about $2\Theta = 30°$. The position and shape of this peak is identical to the peak of films pyrolyzed at only 300 or 350 °C which were found

to be amorphous by TEM. For the "amorphous" films this may indicate a medium range order with structural units similar to those present in the Pb–Ca–Ti–fluorite phase. Similar results, which may point to an increase of order in the "amorphous" phase during low temperature heat treatment (~300 °C) have been proposed for PZT films by high resolution TEM.[21]

The phase transformation from Pb–Ca–Ti–fluorite to PCT perovskite for heating at 1 °C/s occurs between 525 and 550 °C, as shown by XRD and TEM. Even though (111) orientation from bottom electrode nucleation of perovskite dominates, some surface nucleation was found in almost all samples by SEM [Fig. 2(b)] as well as by TEM [Fig. 6(c)], and could be of significant importance for the electrical properties as discussed below. TEM also showed some evidence of nucleation at interfaces between individual stacks of RTA-treated material where the grains do not necessarily have a (111) orientation. An indication for this may be a certain amount of (100)/(001) and (110) orientated grains, as seen by x-ray diffraction, e.g., in Fig. 4.

The reason to obtain strong (111) orientation of the PCT layers is related to the fact that perovskite grows in a locally epitaxial fashion on the 2 nm thick TiO_2 nucleation layer on top of the Pt (111) electrode.[4] This results in the columnar structure of the porous perovskite, as seen by TEM, e.g., in the DF image of Fig. 7(b), as well as by SEM [Fig. 2(b)]. Perovskite (111) nucleates largely at the substrate/film interface, and a growth and phase transformation front of highly (111) oriented perovskite moves toward the surface of the film, consuming the fluorite and incorporating its porosity. A previous study showed a similar phenomenon for the epitaxial growth of $(001)/(100)PbTiO_3$ on single crystal $SrTiO_3$. This resulted in a columnar, porous microstructure where small perovskite grains (previously fluorite) all had the same (100) orientation with a large mosaic spread. Heat treatment at higher temperatures in a PbO-saturated atmosphere allowed reduction of the mosaic spread and densification of the layers.[14]

In the present case, heating to higher temperatures did not result in further densification and the porosity was retained, leading to the low permittivity desired. As the precursors do not contain an excess of lead, this may result from a small lead loss below the detection limit of EDS and RBS (~1–3%), which already can hinder densification.[22] Slow heating, where the films remain relatively long in the stability region of fluorite will contribute to lead loss. The vapor pressure of PbO over PbO at 650 °C, for example, is about 0.4 Pa and thus 1.5 orders of magnitude higher than for PbO over $PbTiO_3$ perovskite, and fluorite should be situated between them.[23–25]

Another phenomenon, related to the Ca content of the layers, could contribute to the retention of the

porosity. TGA/DSC experiments on PCT25 to high temperature have shown that an additional weight loss and the evolution of CO_2 occur at about 720 °C. Other workers have observed the same phenomenon which probably can be attributed to the presence of a small quantity of carbonate.[26] Due to the strong tendency of calcium to form carbonate, a minor amount of it may also be present in the films of this study. The evaporation of lead from the surfaces of individual grains (in the fluorite state, before the phase transformation to perovskite) may cause an excess of Ca on the grain surface which may allow the formation of carbonate. This thin layer of Ca carbonate or a Ca-rich grain-boundary phase could further hinder densification. This is supported by the fact that the high Ca content films studied here tend to have significantly smaller grain sizes than films with no or little calcium (see Fig. 3).

B. Evolution of dense microstructures

Heating at 60 °C/s to 370 °C allowed for observation of columnar perovskite grains, originating at the film/substrate interface, growing into the amorphous matrix, as shown in Fig. 5(b). This direct crystallization has also been observed for PZT.[27] Continued burnout of residual organics in the amorphous phase creates small pores in the rapidly heated material. The high density of these films can be explained only if mechanisms for pore elimination are taking place. The TEM micrograph in Fig. 5(b) shows an array of pores at the interface between the crystallizing perovskite and the amorphous phase.

A likely mechanism for pore elimination is the "pushout" of pores by the advancing crystallization front. While the perovskite crystallization front moves up from the film/substrate interface, vacancies and pores should have the tendency to not be incorporated into the perovskite. Instead they should move with the front and collect at the interface with the amorphous phase where vacancies should have a lower free energy than in perovskite. Generally, the ability of a pore to move with a grain boundary is given by the diffusion of atoms at the pore surface. In single phase material pores may be located on grain boundaries and the driving force for pore mobility, when grain boundaries move during grain growth, is the differential curvature between the leading and trailing surfaces of the pore.[28]

In the case of an amorphous/perovskite interface, the pore mobility could result from two diffusion phenomena. For one, the amorphous phase is at the leading surface of the pore and a higher surface diffusivity of species for the disordered structure of the amorphous phase compared to the ordered perovskite can be expected. Thus, a flux of atoms should move toward the trailing perovskite surface, which enables the pore to move with the advancing crystallization front. Second,

an evaporation/condensation process may take place. The constituents in the amorphous phase are less strongly bound and thus have a higher evaporation rate than in perovskite (especially lead or lead oxide), again resulting in a high mobility of the pores. As stated earlier, the difference between the PbO vapor pressure over PbO and PbO over perovskite is about 1.5 orders of magnitude.[23] Assuming the PbO vapor pressure over the amorphous phase to be similar to the one over PbO, an estimate of the deposition rate by PbO evaporation/condensation onto another surface can be made, resulting in significant rates on the order of 10 monolayers/s ($\sim$ 40 Å/s). Maxwell–Boltzmann gas statistics gives the incidence of molecules on a surface per second to $\phi = p/\sqrt{2\pi m k T}$, where p is the vapor pressure ($\sim$ 0.1 Pa for PbO at $\sim$875 K),[23] m is the molecular mass, k the Boltzmann constant, and T the temperature in Kelvin. This results in about 6×10^{20} molecules/m^2 s. Dividing by the number of molecules/m^2 (unit cell size: $\sim$4 Å) gives about 10 monolayers/s. Due to the high free energy change associated with the transformation of amorphous material to perovskite, the progression of the crystallization front can be expected to be relatively fast.[14,29] According to the estimate above, the pore mobility should be sufficiently high to allow them to move along with the transformation front. Furthermore, due to its exothermic character the direct crystallization from the amorphous phase may cause temperatures higher than the RTA annealing program, further increasing PbO evaporation/condensation.[27,30] SEM demonstrated that the densification must be terminated at about 500 °C because the thickness of the films did not decrease any further during heating to higher temperatures. The diffusion phenomena may also lead to pore shrinkage, depending on the relative velocities of the transformation front and the evaporation/condensation process. For the case of films heated only at 1 °C/s (Sec. B), where the perovskite crystallizes via an intermediate Pb–Ca–Ti–fluorite phase, the free energy difference between fluorite and perovskite can be expected to be much smaller and pore elimination is not likely to occur to the same extent.

C. Electrical properties and microstructure/property relationships

The differences in microstructure obtained for slow or fast heating manifest themselves in the electrical properties of the films, which is shown in Fig. 10(a) for PCT20. The permittivity drops with decreasing heating rate as the volume fraction of porosity in the films increases. The microstructure with reduced permittivity (and heat capacity) can be considered as a matrix-void composite of 3-0 type connectivity.[7]

For porous films heated at 1 °C/s, it was observed that the pyroelectric coefficient does not drop as significantly with decreasing heating rate as seen for ϵ_r [Fig. 10(a)]. This may be related to a layer of dense, probably surface nucleated, perovskite, as observed by SEM [Fig. 2(b)] and TEM [Fig. 6(c)]. If this layer were not present, the films would have highly porous surfaces and thus a proportionally reduced charge density (and consequently a reduced p) as compared to a dense film. Also, porosity may locally remove stress-induced reductions of the pyroelectric coefficient (piezoelectric effect) and facilitate poling of certain (001) oriented grains, further reducing the decrease in p. The film can thus be looked at as a two-layer system. The top layer provides a high pyroelectric coefficient and the bottom layer the low permittivity desired.

With higher Ca contents (PCT25, PCT30) the decrease of p toward slower heating rates becomes more pronounced and at the same time ϵ_r of films heated at 1 °C/s continues to decrease. This may be related to the smaller grain size observed for high Ca compositions and the possibility of Ca-rich surface layers on the grains as suggested before, but further experiments are necessary to confirm this. In PCT ceramics an increasing Ca content increases the polarizability due to the reduction of the c/a ratio. However, for porous films the poling field necessary to achieve a saturated pyroelectric coefficient was found to increase for compositions with high Ca contents. For example 400–500 kV/cm were sufficient for PCT15, whereas higher fields of 700–800 kV/cm were required for PCT25 and PCT30. An explanation may be that domain-wall motion and thus polarizability is significantly reduced in small-grained materials,[31,32] as observed for porous PCT films where the average grain size is decreasing from about $\sim$83 nm for PbTiO$_3$ to $\sim$30 nm for PCT30 (Fig. 3).

Poling experiments showed that a decrease of ϵ_r of $\sim$ 15–20% compared to the unpoled state occurs [Figs. 9(a) and 9(b)]. During poling the number of domains and thus domain walls is reduced (especially 180° domains), and oxygen vacancies as well as defect dipoles interact with the domain walls.[33–36] This will lower the domain-wall contribution to ϵ_r after hot-poling for low ac-field ϵ_r measurements at room temperature, as suggested elsewhere.[20,37,38]

The increase of the figures of merit $F_V = p/\epsilon_r$ for voltage response and $F_D = p/\sqrt{\epsilon_r \tan \delta}$ for detectivity in dependence of the Ca content of the porous films is shown in Fig. 10(b). Combining a high pyroelectric coefficient from Ca substitution with porous microstructures of reduced permittivity and adequate poling procedures results in excellent values of F_V and F_D. The maximum was found for PCT25, where F_V is 3–4 times and F_D 2–3 times higher than recent results on PZT[2,39,40] and PCT.[41]

V. CONCLUSIONS

It was shown that incorporation of porosity into Pb$_{1-x}$Ca$_x$TiO$_3$ pyroelectric thin films can significantly increase the figure of merit by formation of a matrix-void composite with reduced permittivity. Control of nucleation and growth allowed the formation of either dense films by a direct amorphous-to-perovskite transformation or of highly porous layers with the low permittivity desired, where the crystallization of PCT perovskite takes place via an intermediate Pb–Ca–Ti–fluorite phase. XRD and TEM analysis allowed establishment of microstructure/property relationships. The pyroelectric coefficient was increased by reducing the c/a ratio with Ca substitution for Pb. Optimization of the poling procedures allowed maximization of the pyroelectric coefficient, and during poling a further lowering of ϵ_r results due the elimination of domain walls. The obtained values of the figures of merit for voltage response and detectivity make the PCT layers excellent candidates for integration in pyroelectric devices.

ACKNOWLEDGMENTS

REFERENCES

1. R. W. Whatmore, Rep. Prog. Phys. **49**, 1335 (1986).
2. P. Muralt, Rep. Prog. Phys. (in press).
3. T. Ikeda, J. Phys. Soc. Jpn. **13**, 335 (1958).
4. P. Muralt, T. Maeder, L. Sagalowicz, S. Scalese, D. Naumovic, R. G. Agostino, N. Xanthopolus, H. J. Mathieu, L. Patthey, and E. L. Bullock, J. Appl. Phys. **83**, 3835 (1998).
5. A. J. Moulson and J. M. Herbert, *Electroceramics* (Chapman and Hall, London, 1990).
6. P. Muralt, Revue de l'électricité de de l'électronique **9**, 56 (1996).
7. R. Newnham, D. P. Skinner, and L. E. Cross, Mater. Res. Bull. **13**, 525 (1978).
8. A. Seifert, P. Muralt, and N. Setter, in *Proceedings of the 5th International Conference on Electronic Ceramics and Applications, Aveiro, Portugal, 1996* (European Ceramic Society), p. 329.
9. S. R. Gurkovich and J. B. Blum, in *Ultrastructure Processing of Ceramics, Glasses and Composites* (Wiley-Interscience, New York, 1984), p. 152.
10. M. L. Calzada, F. Carmona, R. Sirera, and B. Jimenez, in *Science and Technology of Electroceramic Thin Films* (Kluwer Academic Publishers, The Netherlands, 1995), p. 157.
11. J. B. Blum and S. R. Gurkovich, J. Mater. Sci. **20**, 4479 (1985).
12. T. Tani and D. A. Payne, J. Am. Ceram. Soc. **77**, 1242 (1994).
13. A. P. Wilkinson, J. S. Speck, A. K. Cheetham, S. Natarajan, and J. M. Thomas, Chem. Mater. **6**, 750 (1994).
14. A. Seifert, F. F. Lange, and J. S. Speck, J. Mater. Res. **10**, 680 (1995).
15. C. J. Brinker and G. W. Scherer, *Sol-gel Science. The Physics and Chemistry of Sol-gel Processing* (Academic Press, San Diego, CA, 1990).
16. S. Chewasatn and S. J. Milne, J. Mater. Sci. **32**, 575 (1997).
17. J. L. Tu and S. J. Milne, J. Mater. Res. **11**, 2556 (1996).
18. N. P. Hartley, P. T. Squire, and E. H. Putley, J. Phys. E **5**, 787 (1972).
19. M. Daglish, Int. Ferroelectrics, (in press).
20. A. Seifert, P. Muralt, and N. Setter, Appl. Phys. Lett. **72**, 2409 (1998).
21. C. Lakeman, Ph.D. Thesis, Univ. of Illinois, 1994.
22. A. I. Kingon and B. C. Clark, J. Am. Ceram. Soc. **66**, 256 (1983).
23. H. E. Brown, *Lead Oxide–Properties and Applications* (Int. Lead Zinc Research Organization Inc., New York, 1985).
24. M. A. Subramanian, G. Aravamudan, and G. V. S. Rao, Prog. Solid State Chem. **15**, 55 (1983).
25. C. K. Kwok and S. B. Desu, Appl. Phys. Lett. **60**, 1430 (1992).
26. R. Sirera, M. Malic, M. Kosec, and M. L. Calzada, in *Proceedings of the 5th International Conference on Electronic Ceramics and Applications, Aveiro, Portugal, 1996* (European Ceramic Society), p. 333.
27. H. Hu, C. J. Peng, and S. B. Krupanidhi, Thin Solid Films **223**, 327 (1993).
28. C. H. Hsueh, A. G. Evans, and R. L. Coble, Acta Metall. **30**, 1269 (1982).
29. C. G. Levi, Acta Mater. **46**, 787 (1998).
30. S. V. Krishnaswamy, R. Messier, P. Swab, L. L. Tongson, and K. Vedam, J. Electr. Mater. **10**, 433 (1981).
31. G. Arlt, Ferroelectrics **76**, 451 (1987).
32. G. Arlt and N. A. Pertsev, J. Appl. Phys. **70**, 2283 (1991).
33. K. Carl and K. H. Härdtl, Ferroelectrics **17**, 473 (1978).
34. T. Baiatu, R. Waser, and K-H. Hardtl, J. Am. Ceram. Soc. **73**, 1663 (1990).
35. J. F. Scott, C. A. Araujo, B. M. Melnick, L. D. McMillan, and R. Zuleeg, J. Appl. Phys. **70**, 382 (1991).
36. W. L. Warren, G. E. Pike, K. Vanheusden, D. Dimos, B. A. Tuttle, and J. Robertson, J. Appl. Phys. **79**, 9250 (1996).
37. M. Kohli, P. Muralt, and N. Setter, Appl. Phys. Lett. **72**, 3217 (1998).
38. M. Kohli, A. Seifert, and P. Muralt, Int. Ferroelectrics **22**, 453 (1998).
39. M. Kohli, C. Wuethrich, K. Brooks, B. Willing, M. Forster, P. Muralt, N. Setter, and P. Ryser, Sensors and Actuators A **60**, 147 (1997).
40. N. M. Shorroks, A. Patel, M. J. Walker, and A. D. Parsons, Microelectronic Eng. **29**, 59 (1995).
41. E. Yamaka, H. Watanabe, H. Kimura, H. Kanaya, and H. Ohkuma, J. Vac. Sci. Technol. A **6**, 2921 (1988).